Performance Analysis of Satellite-Vehicle Networks With a Non-Terrestrial Vehicle

Shutong Wang, Liang Yang, Xingwang Li, Kefeng Quo, Hongwu Liu, Houbing Song and Rutvij H. Jhaveri

***Abstract*—In this work, we propose a non-terrestrial vehicle communication network where the communication between the satellite and the terrestrial source is assisted by a unmanned aerial vehicle (UAV) used as a relay. In particular, a reconfigurable intelligent surface (RIS) is used in the RF channel to reflect the signals of the terrestrial user to the relay with a fixed amplification gain, while free-space optical (FSO) is applied to the relay-satellite link to obtain a high speed transmission. For such a dual-hop system, assuming that the FSO channel experiences $\mathcal{M}$-distributed fading with pointing errors, the expressions for the outage probability (OP) and average bit error rate (ABER) are evaluated in closed-forms. In addition, the high signal-to-noise ratio (SNR) analyses for the OP and ABER are developed and the lower and upper bounds on the average channel capacity (ACC) are calculated to obtain further insights. Results show that the diversity order of the proposed system is $\min\{k_w, m_w\}$, where these two parameters are related to the Nakagami-*m* distribution parameters and the number of RIS elements. Finally, we take the shadowing effects into consideration, and it can be seen that the shadowing effects significantly degrade the system performance.**

***Index Terms*—Amplified-and-forward, satellite-vehicle networks, free-space optical, RIS, unmanned aerial vehicle (UAV).**

I. Introduction

With the evolution of communication technologies, Internet of Vehicles (IoV) network will be an important application scenario. IoV utilizes wireless communication technology to achieve network connectivity between vehicles and different terminals (i.e. vehicles, service platforms, people), and provides intelligent and efficient transportation services. Generally, the communication connections between the vehicles and the cloud platforms can be implemented by the conventional mobile cellular systems or the satellite wireless communication. Therefore, owing to its wide coverage and enormous potential to serve countless flights and ground users to meet the explosive growth of global mobile data demand, space-air-ground integrated vehicle network (SAGIVN) has been considered in [1]-[3].

Recently, reconfigurable intelligent surface (RIS) demonstrates the potential to achieve high network energy efficiency requirements [4]. Due to its unique structural characteristics, the RIS can effectively improve the wireless communication environment of the IoV, thereby improving the communication quality of IoV networks. More recently, applying RISs to IoV has received extensive researches [5]-[7]. In [5], the authors studied the RIS-aided unmanned aerial vehicle (UAV) vehicular communication systems with infinite and finite block length codes. In [6], the rate-splitting multiple access scheme for RIS-aided UAV multi-user vehicular communication network with co-channel interference was investigated. In [7], the authors investigated the optimization problem of millimeter-wave communication with link blockages with the help of RISs in IoV. In addition, due to their flexibility, UAVs including drones, balloons, high altitude platform (HAP), low altitude platform (LAP), and quadcopters are extensively used in current wireless communication systems [8]. The UAV+RIS topic also has received extensive attention. For instance, in [9], the authors proposed an RIS-assisted UAV framework, which uses an RIS set on walls to reflect signals to the UAV serving as a relay to retransmit the messages to the destination. In [10], the authors considered applying a buoy serving as a relay to build the communication connection between the UAV and the underwater node.

In the deep space communication environment, RF links are affected by the solar scintillation [11], which results in severe signal fading. Also, the conventional radio frequency (RF) communication is affected by the limited capacity, spectrum congestion, low bandwidth, and regulatory constraints. However, free-space optical (FSO) links are almost immune to the solar scintillation, and has rich spectrum resources, high throughput, low power consumption, and other advantages. Due to its significant advantages, the FSO has been widely applied to the free-space communication, such as the satellite-terrestrial and satellite-satellite communication [12]. However, due to the existence of obstacles such as buildings and trees on the ground, the line-of-sight (LoS) links of FSO communication may be blocked in some urban environments. To address this issue, one can apply the so-called mixed RF/FSO structure where the UAV has a relay on it, the ground user-UAV link is the RF link, while the UAV-satellite link is a FSO link. In [13], the authors considered the mixed FSO-RF communication between the ground and satellites with and without HAP stations. In [14], the performance of a terahertz

Shutong Wang and Liang Yang are with the College of Computer Science and Electronic Engineering, Hunan University, Changsha 410082, China (email:S211000762@hnu.edu.cn, liangy@hnu.edu.cn).

Xingwang Li is with the School of Physics and Electronic Information Engineering, Henan Polytechnic University, Jiaozuo 454000, China (e-mail: lixingwangbupt@gmail.com).

Kefeng Guo is with the School of Space Information, Space Engineering University, Beijing 101407, China (e-mail: guokefeng.cool@163.com).

Hongwu Liu is with the School of Information Science and Electrical Engineering, Shandong Jiaotong University, Jinan 250357, China (e-mail: liuhongwu@sdjtu.edu.cn).

Houbing Song is with the Department of Information Systems, University of Maryland, Baltimore County (UMBC), Baltimore, MD 21250 USA (email: h.song@ieee.org; songh@umbc.edu).

Rutvij H. Jhaveri is with the Department of Computer Science and Engineering, School of Technology, Pandit Deendayal Energy University, Gandhinagar 382007, India (e-mail: rutvij.jhaveri@sot.pdpu.ac.in).

(THz)/FSO hybrid wireless transmission system was studied, taking into account the joint effects of channel fading and pointing errors on the THz and FSO links.

To the authors' knowledge, the performance analysis of the RIS-aided SAGIVN has not been thoroughly studied. Thus, a cooperative satellite-vehicle communication network with the help of a UAV is proposed. For practical considerations, here the UAV can be a LAP or HAP. To further improve the communication quality of the ground vehicle-relay link and expand the coverage, an RIS is used in the first RF link. Specifically, the vehicle source on the ground sends signals to the RIS fixed on the buildings and the RIS reflects the signals to the relay. Then, the relay converts its received electric signals to the optical signals with help of an electric-to-optical (E2O) conversion device. After that, the optical signals are amplified by using a fixed-gain amplifier and retransmitted to the satellite by way of the FSO link, where pointing errors exist in the FSO link. In this work, the main contributions can be summarized as follows:

- A cooperative satellite-vehicle RF/FSO relaying network with the help of a UAV and an RIS is proposed, where the RF and FSO links are modeled using K_G distribution and $\mathcal{M}$-distribution, respectively.
- New formulas for the statistical distributions of the $\mathcal{M}$-distribution are derived.
- The exact expressions of the cumulative distribution function (CDF) and the probability density function (PDF) of the system signal-to-noise ratio (SNR) are derived. Based on these, the exact expressions for the outage probability (OP) and average bit error rate (ABER) are evaluated.
- To obtain more meaningful conclusions, asymptotic analyses of OP and ABER are also presented. In addition, the upper and lower bounds on the average channel capacity (ACC) are calculated to obtain some more useful conclusions.
- The shadowing effects in the RF channels are considered, and the analytical results for the OP and ABER are developed.

A. Organization

The remainder of this paper is organized as follows. The system and channel models are presented in Section II. In Section III, the performance indicators of the system are calculated, including OP, ABER and the upper and lower bounds on ACC. In Section IV, the OP and ABER of the proposed system with the shadowing effects in the RF channels are derived. Numerical evaluated results are presented and discussed in Section V. Finally, in Section VI, the conclusions can be found.

II. System and Channel Models

As depicted in Fig. 1, we study a UAV-aided cooperative satellite-vehicle network, which consists of a vehicle source (S), an RIS employed on a building with N reflective elements, a relay (R) operating under a fixed gain amplify-and-forward (AF) protocol located on a UAV, and a satellite (D). To ensure that the R-D link is relatively static, the UAV can be a LAP or HAP. Further, we assume that all the communication nodes are only deployed with one antenna, and no direct links exist between S and R, and D. The entire signal transmission requires two time slots. In the first stage, the RF signal is sent from S to R with the aid of the RIS. In the second one, after the E2O conversion at R, the optical signal amplified by a fixed gain amplifier is transmitted to D by way of the FSO link. Since S is located on the ground and the signals transmitted from S are easily affected by the rich scatters, such as buildings and trees, we suppose that the S-RIS link follows Rayleigh fading. Besides, owing to the high position of R in the air, we assume that the RIS-R link follows the Nakagami-m fading. Moreover, we focus on the small-scale fading for the RF link, and the angle-of-arrival fluctuation of the UAV and atmospheric attenuation are ignored for the FSO link. In addition, due to the fact that shadowing effect is a log-normal distribution, the system performance evaluation becomes very difficult. Thus, we ignore the shadowed fading for the RF link in this work. This is a reasonable assumption since the RIS and UAV are placed in higher positions and blockage from objects in the signal path seldom happens.

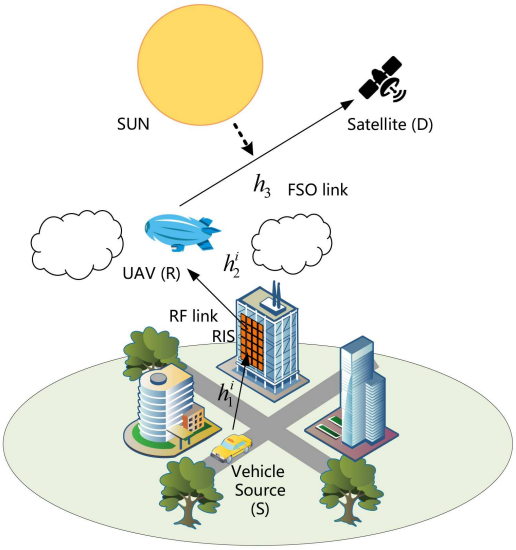

Fig 1. System model.

A. RF link

In the first time slot, S transmits signals to the UAV with the assistance of the RIS and the resulting signal at R is

$$y_1 = \sqrt{L_S L_R}\left[\sum_{i=1}^{N} h_1^i e^{j\phi_i} h_2^i\right] x + n_1. \tag{1}$$

where $h_1^i = \epsilon_i e^{-j\xi_i}$ and $h_2^i = b_i e^{-j\delta_i}$ are the channel gains of the cascaded channels ($i = 1, 2, ..., N$), and ϵ_i and b_i are the channel amplitudes of h_1^i and h_2^i, ξ_i and δ_i represent the phases of h_1^i and h_2^i, respectively. ϵ_i follows a Rayleigh distribution with variance $(4-\pi)/4$ and mean $\sqrt{\pi}/2$, and b_i obeys a Nakagami-m distribution with the fading parameter $m \geq 1/2$. And $n_1 \sim \mathcal{CN}(0, N_1)$ is the additive white Gaussian noise (AWGN). In (1), $L_S = 10^{g_S/10}/r_S^{\mu_S}$ and $L_R = 10^{g_R/10}/r_R^{\mu_R}$

are the large-scale (local average) behaviors of h_1^i and h_2^i [15], respectively, where g_S and g_R are system dependent constants, μ_S and μ_R are the path loss exponents, r_S and r_R are the distance between S and RIS, RIS and R, respectively.

Then, setting $\phi_i = \xi_i + \delta_i$ $(i = 1, 2, ..., N)$, we obtain the SNR at the UAV as

$$\gamma_1 = \frac{L_S L_R E_S \left(\sum_{i=1}^{N} \epsilon_i b_i\right)^2}{N_1} = Z^2 \bar{\gamma}_1, \tag{2}$$

where $Z = \sum_{i=1}^{N} \epsilon_i b_i$, E_S is the average power of the signal and $\bar{\gamma}_1 = L_S L_R E_S / N_1 = 10^{(g_S+g_R)/10} E_S / N_1 r_S^{\mu_S} r_R^{\mu_R}$ is the average SNR of the S-R link. From [9], we apply the K_G distribution to model the statistical distribution of γ_1. Thus, the PDF and CDF of γ_1 are obtained as

$$f_{\gamma_1}(\gamma_1) \approx \frac{2\Xi^{k_w+m_w} \gamma_1^{\left(\frac{k_w+m_w}{2}-1\right)}}{\bar{\gamma}_1^{\frac{k_w+m_w}{2}} \Gamma(k_w)\Gamma(m_w)} K_{k_w-m_w}\left(2\Xi\sqrt{\frac{\gamma_1}{\bar{\gamma}_1}}\right), \tag{3}$$

$$F_{\gamma_1}(\gamma_1) \approx \frac{1}{\Gamma(k_w)\Gamma(m_w)} \mathrm{G}_{1,3}^{2,1}\left(\frac{\Xi^2\gamma_1}{\bar{\gamma}_1}\middle| \begin{matrix} 1 \\ k_w, m_w, 0 \end{matrix}\right), \tag{4}$$

where the definitions of the parameters $k_w = \frac{-b_w+\sqrt{b_w^2-4a_w c_w}}{2a_w}$, $m_w = \frac{-b_w-\sqrt{b_w^2-4a_w c_w}}{2a_w}$, a_w, b_w, and c_w can be found in [16]. $\Xi = \sqrt{\frac{k_w m_w}{\Omega_w}}$, and Ω_w is the mean power of Z. Moreover, $K_v(\cdot)$ is the modified v-order Bessel function of the second kind, $\Gamma(\cdot)$ is the gamma function, and $\mathrm{G}_{\cdot,\cdot}^{\cdot,\cdot}(\cdot|)$ is the Meijer G-function.

B. FSO link

Similar to [17], a subcarrier intensity modulation (SIM) mode is applied to implement the E2O conversion. For the FSO link, the M fading model is applied to model the turbulence. In addition, pointing errors are also taken into consideration. Then, from [17, Eq. (4)], we have

$$y_2 = \sqrt{E_r} G h_3 (1 + \eta y_1) + n_2, \tag{5}$$

where $n_2 \sim \mathcal{CN}(0, N_2)$ is the AWGN of the FSO link, E_r is the transmit power of R, G is the amplification gain, and η is the E2O conversion coefficient. In addition, $h_3 = h_a h_p$ is the FSO channel gain composed of two attenuation components due to the turbulence-induced fading and pointing errors. Finally, after filtering out the direct-current component, y_2 is rewritten as

$$y_2 = \sqrt{E_r} G h_3 \eta y_1 + n_2. \tag{6}$$

In [18], the PDF of the optical channel gain taking into account pointing errors has been given. However, for the convenience of subsequent calculation, we change Eq. (18) given in [18] to another form. By using [19, Eq. (2.6.20)], the Bessel-K function [18, Eq. (18)] can be rewritten as

$$\begin{aligned} K_{\alpha-k}(2\sqrt{\theta h_a}) =& \frac{2^{\alpha+k-2}}{\pi} (\theta h_a)^{-\frac{\alpha+k}{2}} \\ & \times \mathrm{G}_{0,4}^{4,0}\left(\frac{\theta^2 h_a^2}{16}\middle| \begin{matrix} - \\ \frac{\alpha}{2}, \frac{\alpha+1}{2}, \frac{k}{2}, \frac{k+1}{2} \end{matrix}\right). \end{aligned} \tag{7}$$

Thus, by applying equations [20, Eq. (07.34.21.0085.01)] and [20, Eq. (07.34.21.0084.01)], the PDF and CDF of h_3 can be rewritten as

$$\begin{aligned} f_{h_3}(h) =& \sum_{k=1}^{\beta} \frac{2^{\alpha+k-3} g^2 A}{\pi h} a_k \theta^{-\frac{\alpha+k}{2}} \\ & \times \mathrm{G}_{2,6}^{6,0}\left(\frac{\theta^2 h^2}{16A_0^2}\middle| \begin{matrix} \frac{g^2+1}{2}, \frac{g^2}{2}+1 \\ \frac{g^2}{2}, \frac{g^2+1}{2}, \frac{\alpha}{2}, \frac{\alpha+1}{2}, \frac{k}{2}, \frac{k+1}{2} \end{matrix}\right), \end{aligned} \tag{8}$$

$$\begin{aligned} F_{h_3}(h) =& \int_0^h f_h(h) dh = \sum_{k=1}^{\beta} \frac{2^{\alpha+k-4} g^2 A}{\pi} a_k \theta^{-\frac{\alpha+k}{2}} \\ & \times \mathrm{G}_{4,8}^{6,2}\left(\frac{\theta^2 h^2}{16A_0^2}\middle| \begin{matrix} \frac{1}{2}, 1, \frac{g^2+1}{2}, \frac{g^2}{2}+1 \\ \frac{g^2}{2}, \frac{g^2+1}{2}, \frac{\alpha}{2}, \frac{\alpha+1}{2}, \frac{k}{2}, \frac{k+1}{2}, 0, \frac{1}{2} \end{matrix}\right), \end{aligned} \tag{9}$$

where $\theta = \alpha\beta/(\omega\beta + \Omega')$, $A = \frac{2\alpha^{\alpha/2}}{\omega^{\alpha/2+1}\Gamma(\alpha)} \left(\frac{\omega\beta}{\omega\beta+\Omega'}\right)^{\beta+\alpha/2}$, $a_k = \binom{\beta-1}{k-1} \frac{(\omega\beta+\Omega')^{1-k/2}}{(k-1)!} \left(\frac{\Omega'}{\omega}\right)^{k-1} \left(\frac{\alpha}{\beta}\right)^{k/2}$, α is a positive parameter related to the effective number of large-scale cells of the scattering process, $\beta = E^2[X]/Var[X]$ is the amount of fading parameter, where X is a variable that follows a gamma distribution, $E[X]$ is the mean and $Var[X]$ is the variance. Similar to [17], [18], we assume that β is an integer. Besides, $\omega = 2b_0(1-\rho)$, $\Omega' = \Omega + \rho 2b_0 + 2\sqrt{2b_0\Omega\rho}\cos(\phi_A - \phi_B)$ denotes the average power of the coherent contributions, and the above parameters are all defined in [17]. Note that values of g represent the degree of influence of pointing errors and $g \to \infty$ corresponds to the non-pointing error case.

Then, we readily have

$$\gamma_2 = h_3^2 \bar{\gamma}_2. \tag{10}$$

where $\bar{\gamma}_2 = E_r \eta^2 / N_2$. Substituting (10) into (8) and (9), we obtain

$$\begin{aligned} f_{\gamma_2}(\gamma_2) =& \sum_{k=1}^{\beta} \frac{2^{\alpha+k-4} g^2 A}{\pi\gamma_2} a_k \theta^{-\frac{\alpha+k}{2}} \\ & \times \mathrm{G}_{2,6}^{6,0}\left(\frac{\theta^2\gamma_2}{16A_0^2\bar{\gamma}_2}\middle| \begin{matrix} \frac{g^2+1}{2}, \frac{g^2}{2}+1 \\ \frac{g^2}{2}, \frac{g^2+1}{2}, \frac{\alpha}{2}, \frac{\alpha+1}{2}, \frac{k}{2}, \frac{k+1}{2} \end{matrix}\right), \end{aligned} \tag{11}$$

$$\begin{aligned} F_{\gamma_2}(\gamma_2) =& \sum_{k=1}^{\beta} \frac{2^{\alpha+k-4} g^2 A}{\pi} a_k \theta^{-\frac{\alpha+k}{2}} \\ & \times \mathrm{G}_{4,8}^{6,2}\left(\frac{\theta^2\gamma_2}{16A_0^2\bar{\gamma}_2}\middle| \begin{matrix} \frac{1}{2}, 1, \frac{g^2+1}{2}, \frac{g^2}{2}+1 \\ \frac{g^2}{2}, \frac{g^2+1}{2}, \frac{\alpha}{2}, \frac{\alpha+1}{2}, \frac{k}{2}, \frac{k+1}{2}, 0, \frac{1}{2} \end{matrix}\right). \end{aligned} \tag{12}$$

C. End-to-End Statistical Distribution

Regarding the fixed-gain relaying mode, the SNR γ_0 of the whole system is written as

$$\gamma_0 = \frac{\gamma_1\gamma_2}{\gamma_2 + C}, \tag{13}$$

where C is a constant related to G. Then, the CDF of γ_0 can be expressed as [10], [21]

$$F_{\gamma_0}(\gamma) = F_{\gamma_1}(\gamma) + \underbrace{\int_0^{\infty} F_{\gamma_2}\left(\frac{C\gamma}{x}\right) f_{\gamma_1}(\gamma + x) dx}_{D_1}. \tag{14}$$

$$F_{\gamma_0}(\gamma)=\frac{1}{\Gamma(k_w)\Gamma(m_w)}\mathrm{G}_{1,3}^{2,1}\left(\frac{\Xi^2\gamma}{\bar{\gamma}_1}\middle|\begin{matrix}1\\k_w,m_w,0\end{matrix}\right)+\sum_{k=1}^{\beta}\frac{2^{\alpha+k-4}g^2Aa_k\theta^{-\frac{\alpha+k}{2}}}{\pi\Gamma(k_w)\Gamma(m_w)}\sum_{i=0}^{\infty}\frac{(-\Xi^2)^i}{i!\bar{\gamma}_1^i}\gamma^i\mathrm{G}_{5,11}^{9,2}\left(\frac{\Xi^2\theta^2C\gamma}{16A_0^2\bar{\gamma}_1\bar{\gamma}_2}\middle|\begin{matrix}\frac{1}{2},1,1-i,\frac{g^2+1}{2},\frac{g^2}{2}+1\\1,\frac{g^2}{2},\frac{g^2+1}{2},\frac{\alpha}{2},\frac{\alpha+1}{2},\frac{k}{2},\frac{k+1}{2},k_w-i,m_w-i,0,\frac{1}{2}\end{matrix}\right). \tag{15}$$

$$\bar{P}_e=\frac{q^p}{2\Gamma(p)}\int_0^{\infty}\gamma^{p-1}e^{-q\gamma}F_{\gamma_0}(\gamma)d\gamma=\frac{1}{2\Gamma(p)\Gamma(k_w)\Gamma(m_w)}\mathrm{G}_{2,3}^{2,2}\left(\frac{\Xi^2}{q\bar{\gamma}_1}\middle|\begin{matrix}1-p,1\\k_w,m_w,0\end{matrix}\right)+\sum_{k=1}^{\beta}\frac{2^{\alpha+k-5}g^2Aa_k\theta^{-\frac{\alpha+k}{2}}}{\pi\Gamma(p)\Gamma(k_w)\Gamma(m_w)}\sum_{i=1}^{\infty}\frac{(-\Xi^2)^i}{i!\bar{\gamma}_1^iq^i}\mathrm{G}_{6,11}^{9,3}\left(\frac{\Xi^2\theta^2C\gamma}{16A_0^2\bar{\gamma}_1\bar{\gamma}_2q}\middle|\begin{matrix}1-p-i,\frac{1}{2},1,1-i,\frac{g^2+1}{2},\frac{g^2}{2}+1\\1,\frac{g^2}{2},\frac{g^2+1}{2},\frac{\alpha}{2},\frac{\alpha+1}{2},\frac{k}{2},\frac{k+1}{2},k_w-i,m_w-i,0,\frac{1}{2}\end{matrix}\right). \tag{19}$$

By substituting (3), (4) and (12) into (14) and applying the equations [20, Eq. (07.34.16.0002.01)] and [20, Eq. (07.34.21.0082.01)], the CDF of γ_0 is obtained and shown as (15) at the top of 3-rd page.

III. Performance Analysis

Next the exact expressions for the OP and ABER of our proposed system are derived. To obtain more insights, we develop the asymptotic representations of OP and ABER at high SNRs. Besides, the upper and lower bounds on the ACC are provided.

A. OP

1) *Exact Analysis:* OP is defined as the probability that the instantaneous SNR γ_0 falling to a given threshold γ_{th}. Thus, it is readily to obtain the OP expression as

$$P_{out}=\Pr(\gamma_0<\gamma_{th})=F_{\gamma_0}(\gamma_{th}). \tag{16}$$

2) *Asymptotic Analysis:* By letting $\bar{\gamma}_1=\bar{\gamma}_2=\bar{\gamma}\to\infty$, the asymptotic representation of the OP is obtained as

$$P_{out}^{\infty}\approx F_{\gamma_1}^{\infty}+D_1^{\infty}. \tag{17}$$

By using [20, Eq. (07.34.06.0040.01)], [20, Eq. (07.34.21.0086.01)] and [22, Eq. 3.381.4], P_{out}^{∞} can be written as

$$P_{out}^{\infty}\approx F_{\gamma_1}^{\infty}+D_1^{\infty}=\frac{\Gamma(|m_w-k_w|)(\Xi^2\gamma_{th})^v}{v\Gamma(k_w)\Gamma(m_w)\bar{\gamma}^v}+\frac{\Gamma(|m_w-k_w|)(\Xi^2\gamma_{th})^v}{\Gamma(k_w)\Gamma(m_w)}\sum_{k=1}^{\beta}\frac{2^{\alpha+k-4}g^2A}{\pi\Gamma(1-v)}a_k\theta^{-\frac{\alpha+k}{2}}\times\sum_{n=1}^{7}\frac{\prod_{j=1,j\neq n}^{7}\Gamma(d_j-d_n)\prod_{j=1}^{3}\Gamma(1-c_j+d_n)}{\prod_{j=4}^{5}\Gamma(c_j-d_n)\prod_{j=8}^{9}\Gamma(1-d_j+d_n)}\times\left(\frac{\theta^2C}{16A_0^2}\right)^{d_n}\left(\frac{1}{\bar{\gamma}}\right)^{v+d_n}, \tag{18}$$

where $[c_1,...,c_5]=[v+1,\frac{1}{2},1,\frac{g^2+1}{2},\frac{g^2}{2}+1]$, $[d_1,...,d_9]=[1,\frac{g^2}{2},\frac{g^2+1}{2},\frac{\alpha}{2},\frac{\alpha+1}{2},\frac{k}{2},\frac{k+1}{2},0,\frac{1}{2}]$ and $v=\min\{k_w,m_w\}$. From (18), since α, k and g are all positive numbers, we obtain the diversity order (DO) of our proposed system as $G_d=v=\min\{k_w,m_w\}$. As k_w and m_w are related to the values of N and m, one can see that the DO is only dependent on the RF link and this observation will be demonstrated in section IV.

B. ABER

1) *Exact Analysis:* By applying [20, Eq. (07.34.21.0088.01)], the ABER for different binary modulation schemes is expressed as (19) shown at the top of the 3-rd page, where p and q are the parameters depended on the modulation scheme.

2) *Asymptotic Analysis:* Letting $\bar{\gamma}_1=\bar{\gamma}_2=\bar{\gamma}\to\infty$, we have

$$\bar{P}_e^{\infty}=\frac{q^p}{2\Gamma(p)}\int_0^{\infty}\gamma^{p-1}e^{-q\gamma}F_{\gamma_0}^{\infty}(\gamma)d\gamma=\frac{\Gamma(|m_w-k_w|)\Gamma(v+p)\Xi^{2v}}{2v\Gamma(p)\Gamma(k_w)\Gamma(m_w)q^v\bar{\gamma}^v}+\frac{\Gamma(|m_w-k_w|)\Gamma(v+p)\Xi^{2v}}{\Gamma(p)\Gamma(k_w)\Gamma(m_w)q^v}\sum_{k=1}^{\beta}\frac{2^{\alpha+k-5}g^2A}{\pi\Gamma(1-v)}a_k\theta^{-\frac{\alpha+k}{2}}\times\sum_{n=1}^{7}\frac{\prod_{j=1,j\neq n}^{7}\Gamma(d_j-d_n)\prod_{j=1}^{3}\Gamma(1-c_j+d_n)}{\prod_{j=4}^{5}\Gamma(c_j-d_n)\prod_{j=8}^{9}\Gamma(1-d_j+d_n)}\times\left(\frac{\theta^2C}{16A_0^2}\right)^{d_n}\left(\frac{1}{\bar{\gamma}}\right)^{v+d_n}. \tag{20}$$

Again, the DO is $G_d=v=\min\{k_w,m_w\}$.

C. ACC

Unfortunately, the exact ACC analysis is very difficult. Therefore, we only provide upper and lower bounds analyses.

1) *Upper Bound:* With the help of [23, Eq. (23)], by utilizing the Jensen's inequality, an upper bound on the ACC is written as

$$\bar{C}=E[\log_2(1+\gamma_0)]\leq\log_2[1+E(\gamma_0)]=\bar{C}_{UB}. \tag{21}$$

Since γ_1 and γ_2 are independent random variables, $E(\gamma_0)$ can be rewritten as

$$E(\gamma_0)=E\left(\frac{\gamma_1\gamma_2}{\gamma_2+C}\right)=E(\gamma_1)E\left(\frac{\gamma_2}{\gamma_2+C}\right), \tag{22}$$

where $E(\gamma_1)$ and $E\left(\frac{\gamma_2}{\gamma_2+C}\right)$ can be derived with the help of [20, Eq. (03.04.21.0116.01)] and [20, Eq. (07.34.21.0086.01)]:

$$E(\gamma_1) = \int_0^\infty \gamma_1 f_{\gamma_1}(\gamma_1) d\gamma_1 = \frac{k_w m_w \bar{\gamma}_1}{\Xi^2}, \tag{23}$$

$$\begin{aligned} E\left(\frac{\gamma_2}{\gamma_2+C}\right) &= \sum_{k=1}^{\beta} \frac{2^{\alpha+k-4} g^2 A}{\pi} a_k \theta^{-\frac{\alpha+k}{2}} \\ &\times \mathrm{G}_{3,7}^{7,1}\left(\frac{\theta^2 C}{16 A_0^2 \bar{\gamma}_2}\middle| \begin{matrix} 0, \frac{g^2+1}{2}, \frac{g^2}{2}+1 \\ 0, \frac{g^2}{2}, \frac{g^2+1}{2}, \frac{\alpha}{2}, \frac{\alpha+1}{2}, \frac{k}{2}, \frac{k+1}{2} \end{matrix}\right). \end{aligned} \tag{24}$$

Based on (19) and (20), $\bar{C}_{UB}$ can be obtained. For $\bar{\gamma}_1 = \bar{\gamma}_2 = \bar{\gamma} \to \infty$, applying [20, Eq. (07.34.06.0040.01)], we have

$$\begin{aligned} \bar{C}_{UB}^{\infty} &= \log_2(E(\gamma_1)) + \log_2(E(\gamma_2)) - \log_2(E(\gamma_2+C)) \\ &\to \log_2(\bar{\gamma}) - \log_2(\Xi^2) + \log_2(k_w) + \log_2(m_w) \\ &+ \log_2\left(\sum_{k=1}^{\beta} \frac{2^{\alpha+k-4} g^2 A}{\pi} a_k \theta^{-\frac{\alpha+k}{2}}\right. \\ &\times \sum_{n=1}^{7} \frac{\prod_{j=1, j\neq n}^{7} \Gamma(q_j - q_n) \prod_{j=1}^{1} \Gamma(1 - p_j + q_n)}{\prod_{j=2}^{3} \Gamma(p_j - q_n)} \\ &\left.\times \left(\frac{\theta^2 C}{16 A_0^2}\right)^{q_n} \left(\frac{1}{\bar{\gamma}}\right)^{q_n}\right), \end{aligned} \tag{25}$$

where $[p_1, p_2, p_3] = [0, \frac{g^2+1}{2}, \frac{g^2}{2}+1]$, $[q_1, ..., q_7] = [0, \frac{g^2}{2}, \frac{g^2+1}{2}, \frac{\alpha}{2}, \frac{\alpha+1}{2}, \frac{k}{2}, \frac{k+1}{2}]$.

2) *Lower Bound:* With the help of [24, Eq. (16)], a tight lower bound on the ACC is expressed as

$$\bar{C} \geq \log_2[1 + e^{E(\ln\gamma_1) + E(\ln\gamma_2) - E(\ln(\gamma_2+C))}] = \bar{C}_{LB}. \tag{26}$$

Using [25, Eq. (2.16.20.1)], we have $E(\ln\gamma_1) = \psi(k_w)\psi(m_w) - 2\ln(\Xi/\sqrt{\bar{\gamma}_1})$, where $\psi(\cdot)$ is the digamma function. Let $E(\ln\gamma_2) - E(\ln(\gamma_2 + C)) = -E(\ln(1 + C/\gamma_2)) = -\lambda$. By using [25, Eq. (8.4.6.5)], [20, Eq. (07.34.16.0002.01)], and [20, Eq. (07.34.21.0013.01)], λ can be obtained

$$\begin{aligned} \lambda &= E\left[\mathrm{G}_{2,2}^{2,1}\left(\frac{\gamma_2}{C}\middle| \begin{matrix} 0, 1 \\ 0, 0 \end{matrix}\right)\right] = \sum_{k=1}^{\beta} \frac{2^{\alpha+k-4} g^2 A}{\pi} a_k \theta^{-\frac{\alpha+k}{2}} \\ &\times \mathrm{G}_{4,8}^{7,2}\left(\frac{\theta^2 C}{16 A_0^2 \bar{\gamma}_2}\middle| \begin{matrix} 1, 1, \frac{g^2+1}{2}, \frac{g^2}{2}+1 \\ \frac{g^2}{2}, \frac{g^2+1}{2}, \frac{\alpha}{2}, \frac{\alpha+1}{2}, \frac{k}{2}, \frac{k+1}{2}, 1, 0 \end{matrix}\right). \end{aligned} \tag{27}$$

For $\bar{\gamma}_1 = \bar{\gamma}_2 = \bar{\gamma} \to \infty$, by applying [20, Eq. (07.34.06.0040.01)], $\bar{C}_{LB}^{\infty}$ is obtained as

$$\begin{aligned} \bar{C}_{LB}^{\infty} &= \frac{E(\ln\gamma_1) + E(\ln\gamma_2) - E(\ln(\gamma_2+C))}{\ln 2} \\ &\to \log_2(\bar{\gamma}) - \log_2(\Xi^2) + \frac{\psi(k_w) + \psi(m_w)}{\ln 2} \\ &- \sum_{k=1}^{\beta} \frac{2^{\alpha+k-4} g^2 A}{\pi \ln 2} a_k \theta^{-\frac{\alpha+k}{2}} \\ &\times \left(\sum_{n=1}^{7} \frac{\prod_{j=1, j\neq n}^{7} \Gamma(w_j - w_n) \prod_{j=1}^{2} \Gamma(1 - u_j + w_n)}{\prod_{j=3}^{4} \Gamma(u_j - w_n) \prod_{j=8}^{8} \Gamma(1 - w_j + w_n)}\right. \\ &\left.\times \left(\frac{\theta^2 C}{16 A_0^2}\right)^{w_n} \left(\frac{1}{\bar{\gamma}}\right)^{w_n}\right), \end{aligned} \tag{28}$$

where $[u_1, ..., u_4] = [1, 1, \frac{g^2+1}{2}, \frac{g^2}{2}+1]$, $[w_1, ..., w_8] = [\frac{g^2}{2}, \frac{g^2+1}{2}, \frac{\alpha}{2}, \frac{\alpha+1}{2}, \frac{k}{2}, \frac{k+1}{2}, 1, 0]$.

From the above high SNR bound analysis, one can see that the system capacity more depends on the RF link. In addition, it can be seen that λ increases when g increases.

IV. Extension to the System with Shadowing Effects in the RF Channels

In this section, we take the shadowing effects into consideration. In practical scenarios, signals experience the shadowed fading during the propagation, which is a kind of the large-scale fluctuation caused by slow changes in local average power levels over long propagation distances due to terrain features, such as buildings and hills [26].

With the consideration of the shadowing effects, the SNR of the RF link can be rewritten as

$$\gamma_1^s = \frac{E_S\left(\sum_{i=1}^{N} s\epsilon_i b_i\right)^2}{r_S^{\mu_S} r_R^{\mu_R} N_1} = Z_1 Z_2 \bar{\gamma}_1^s, \tag{29}$$

where s denotes the shadowing effect, which is widely characterized by a lognormal distribution. Besides, $\bar{\gamma}_1^s = \frac{E_S}{r_S^{\mu_S} r_R^{\mu_R} N_1}$, $Z_1 = s^2$, $Z_2 = \left(\sum_{i=1}^{N} \epsilon_i b_i\right)^2$. Since $10\log_{10} s \sim \mathcal{N}(0, \sigma_1^2)$, the PDF of s can be obtained as [27]

$$f_s(s) = \frac{10 e^{-\frac{(10\log_{10} s)^2}{2\sigma_1^2}}}{10\ln 10 \sqrt{2\pi}\sigma_1 s}. \tag{30}$$

where σ_1 is the standard deviation of $10\log_{10} s$. Applying eq. (30) to evaluate the system performance is generally very difficult. Thus, for a tractable analysis, many works using the gamma distribution to approximate the lognormal distribution, like [18], [28], [29]. Then, the PDF of s can be represented as

$$f_s(s) = \frac{s^{v_1 - 1}}{\Gamma(v_1) \lambda_1^{v_1}} e^{\frac{s}{\lambda_1}}, \tag{31}$$

where $v_1 = \frac{1}{e^{\sigma_1^2} - 1}$ inversely reflects the shadowing severity and $\lambda_1 = (e^{\sigma_1^2} - 1) e^{\frac{\sigma_1^2}{2}}$ [29]. $\varsigma_1 = v_1 \lambda_1$ is the gamma shadow area mean power. Meanwhile, according to the developed method in [30] and similar to the RIS-related works [31]-[33], we approximate $Z = \sum_{i=1}^{N} \epsilon_i b_i$ to a gamma distribution. Thus, we can write the PDF expressions of $Z_1 = s^2$ and $Z_2 = Z^2$ as

$$f_{Z_n}(z_n) = \frac{z_n^{\frac{v_n}{2} - 1}}{2\Gamma(v_n) \lambda_n^{v_n}} e^{-\frac{\sqrt{z_n}}{\lambda_n}}. \tag{32}$$

where n={1,2}, $v_2 = \frac{E(Z)^2}{VAR(Z)}$ and $\lambda_2 = \frac{VAR(Z)}{E(Z)}$. After some mathematical computation, $E(Z)$ and $VAR(Z)$ can be written as

$$E(Z) = N \frac{\sqrt{\pi}\Gamma\left(m + \frac{1}{2}\right)}{2\sqrt{m}\Gamma(m)}, \tag{33}$$

$$VAR(Z) = N\left[1 - \frac{\pi\Gamma\left(m + \frac{1}{2}\right)^2}{4m\Gamma(m)^2}\right]. \tag{34}$$

$$F_{\gamma_0^s}(\gamma)=\frac{2^{v_1+v_2-2}}{\pi\Gamma(v_1)\Gamma(v_2)}\mathrm{G}_{1,5}^{4,1}\left(\frac{\gamma}{16\lambda_1^2\lambda_2^2\bar{\gamma}_1^s}\middle|\begin{matrix}1\\ \frac{v_1}{2},\frac{v_1+1}{2},\frac{v_2}{2},\frac{v_2+1}{2},0\end{matrix}\right)+\sum_{k=1}^{\beta}\frac{2^{\alpha+k+v_1+v_2-6}g^2Aa_k\theta^{-\frac{\alpha+k}{2}}}{\pi^2\Gamma(v_1)\Gamma(v_2)}$$
$$\times\sum_{i=0}^{\infty}\frac{(-\gamma)^i}{i!(16\lambda_1^2\lambda_2^2\bar{\gamma}_1^s)^i}\mathrm{G}_{5,13}^{11,2}\left(\frac{\theta^2C\gamma}{256A_0^2\lambda_1^2\lambda_2^2\bar{\gamma}_1^s\bar{\gamma}_2}\middle|\begin{matrix}\frac{1}{2},1,1-i,\frac{g^2+1}{2},\frac{g^2}{2}+1\\ 1,\frac{g^2}{2},\frac{g^2+1}{2},\frac{\alpha}{2},\frac{\alpha+1}{2},\frac{k}{2},\frac{k+1}{2},\frac{v_1}{2}-i,\frac{v_1+1}{2}-i,\frac{v_2}{2}-i,\frac{v_2+1}{2}-i,0,\frac{1}{2}\end{matrix}\right) \tag{38}$$

$$\bar{P}_e^s=\frac{q^p}{2\Gamma(p)}\int_0^{\infty}\gamma^{p-1}e^{-q\gamma}F_{\gamma_0^s}(\gamma)d\gamma=\frac{2^{v_1+v_2-3}}{\pi\Gamma(v_1)\Gamma(v_2)\Gamma(p)}\mathrm{G}_{2,5}^{4,2}\left(\frac{1}{16\lambda_1^2\lambda_2^2\bar{\gamma}_1^s}\middle|\begin{matrix}1-p,1\\ \frac{v_1}{2},\frac{v_1+1}{2},\frac{v_2}{2},\frac{v_2+1}{2},0\end{matrix}\right)$$
$$+\sum_{k=1}^{\beta}\frac{2^{\alpha+k+v_1+v_2-7}g^2Aa_k\theta^{-\frac{\alpha+k}{2}}}{\pi^2\Gamma(v_1)\Gamma(v_2)\Gamma(p)}\sum_{i=0}^{\infty}\frac{(-1)^i}{i!(16\lambda_1^2\lambda_2^2\bar{\gamma}_1^sq)^i} \tag{40}$$
$$\times\mathrm{G}_{6,13}^{11,3}\left(\frac{\theta^2C}{256A_0^2\lambda_1^2\lambda_2^2\bar{\gamma}_1^s\bar{\gamma}_2q}\middle|\begin{matrix}1-p-i,\frac{1}{2},1,1-i,\frac{g^2+1}{2},\frac{g^2}{2}+1\\ 1,\frac{g^2}{2},\frac{g^2+1}{2},\frac{\alpha}{2},\frac{\alpha+1}{2},\frac{k}{2},\frac{k+1}{2},\frac{v_1}{2}-i,\frac{v_1+1}{2}-i,\frac{v_2}{2}-i,\frac{v_2+1}{2}-i,0,\frac{1}{2}\end{matrix}\right)$$

By using [18, Eq. (2.6.20)], [20, Eq. (07.34.16.0001.01)], [20, Eq. (07.34.21.0084.01)], and [22, Eq. (3.471.9)], the PDF and CDF of the SNR γ_1^s for the RF link in the presence of the shadowing effects can be rewritten as

$$f_{\gamma_1^s}(\gamma_1)=\int_0^{\infty}\frac{1}{z_1\bar{\gamma}_1^s}f_{Z_1}(z_1)f_{Z_2}\left(\frac{\gamma_1}{z_1\bar{\gamma}_1^s}\right)dz_1$$
$$=\frac{2^{v_1+v_2-2}}{16\pi\Gamma(v_1)\Gamma(v_2)\lambda_1^2\lambda_2^2\bar{\gamma}_1^s} \tag{35}$$
$$\times\mathrm{G}_{0,4}^{4,0}\left(\frac{\gamma_1}{16\lambda_1^2\lambda_2^2\bar{\gamma}_1^s}\middle|\begin{matrix}-\\ \frac{v_1}{2}-1,\frac{v_1-1}{2},\frac{v_2}{2}-1,\frac{v_2-1}{2}\end{matrix}\right),$$

$$F_{\gamma_1^s}(\gamma_1)=\int_0^{\gamma_1}f_{\gamma_1^s}(\gamma_1)d\gamma_1=\frac{2^{v_1+v_2-2}}{\pi\Gamma(v_1)\Gamma(v_2)}$$
$$\times\mathrm{G}_{1,5}^{4,1}\left(\frac{\gamma_1}{16\lambda_1^2\lambda_2^2\bar{\gamma}_1^s}\middle|\begin{matrix}1\\ \frac{v_1}{2},\frac{v_1+1}{2},\frac{v_2}{2},\frac{v_2+1}{2},0\end{matrix}\right). \tag{36}$$

Then, the CDF of the e2e SNR γ_0^s can be expressed as

$$F_{\gamma_0^s}(\gamma)=F_{\gamma_1^s}(\gamma)+\int_0^{\infty}F_{\gamma_2}\left(\frac{C\gamma}{x}\right)f_{\gamma_1^s}(\gamma+x)dx. \tag{37}$$

By substituting (12), (35), and (36) into (37) and with the help of [20, Eq. (07.34.16.0002.01)], [20, Eq. (07.34.21.0082.01)], and [22, Eq. (3.381.4)], the CDF of γ_0 is obtained and shown as (38) at the top of this page.

From (38), the OP is $P_{out}^s=F_{\gamma_0^s}(\gamma_{th})$. Let $\bar{\gamma}=\bar{\gamma}_1=\bar{\gamma}_2\to\infty$, by applying [20, Eq. (07.34.06.0040.01)], the asymptotic expression for the OP can be obtained as

$$P_{out}^{s\infty}\approx\frac{2^{v_1+v_2-1}\Gamma\left(\frac{|v_2-v_1|}{2}\right)\Gamma\left(\frac{|v_2-v_1|+1}{2}\right)\gamma_{th}^{\frac{u}{2}}}{\sqrt{\pi}\Gamma(v_1)\Gamma(v_2)(16\lambda_1^2\lambda_2^2q)^{\frac{u}{2}}u\bar{\gamma}^{\frac{u}{2}}}$$
$$+\sum_{k=1}^{\beta}\frac{2^{\alpha+k+v_1+v_2-6}g^2A\Gamma\left(\frac{|v_2-v_1|}{2}\right)\Gamma\left(\frac{|v_2-v_1|+1}{2}\right)\gamma_{th}^{\frac{u}{2}}}{\pi^{\frac{3}{2}}\Gamma(v_1)\Gamma(v_2)(16\lambda_1^2\lambda_2^2q)^{\frac{u}{2}}\Gamma\left(1-\frac{u}{2}\right)}$$
$$\times a_k\theta^{-\frac{\alpha+k}{2}}\left(\frac{\theta^2C}{16A_0^2}\right)^{\varrho_n}\left(\frac{1}{\bar{\gamma}}\right)^{\frac{u}{2}+\varrho_n}$$
$$\times\sum_{n=1}^{7}\frac{\prod_{j=1,j\neq n}^{7}\Gamma(\varrho_j-\varrho_n)\prod_{j=1}^{3}\Gamma(1-\varpi_j+\varrho_n)}{\prod_{j=4}^{5}\Gamma(\varpi_j-\varrho_n)\prod_{j=8}^{9}\Gamma(1-\varrho_j+\varrho_n)}, \tag{39}$$

where $[\varpi_1,...,\varpi_5]=[\frac{u}{2}+1,\frac{1}{2},1,\frac{g^2+1}{2},\frac{g^2}{2}+1]$, $[\varrho_1,...,\varrho_9]=[1,\frac{g^2}{2},\frac{g^2+1}{2},\frac{\alpha}{2},\frac{\alpha+1}{2},\frac{k}{2},\frac{k+1}{2},0,\frac{1}{2}]$, $u=\min\{v_1,v_2\}$. Then, we can obtain the DO of the system as $G_d^s=\frac{u}{2}=\frac{1}{2}\min\{v_1,v_2\}$, where v_2 is related to the values of N and m. The same conclusion can be drawn that the DO is only dependent on the RF link.

Similarly, by applying [20, Eq. (07.34.21.0088.01)], the ABER for different binary modulation schemes is expressed as (40) shown at the top of this page. Again, when $\bar{\gamma}=\bar{\gamma}_1=\bar{\gamma}_2\to\infty$, the asymptotic expression for the ABER can be written as

$$\bar{P}_e^{s\infty}\approx\frac{2^{v_1+v_2-2}\Gamma\left(\frac{|v_2-v_1|}{2}\right)\Gamma\left(\frac{|v_2-v_1|+1}{2}\right)\Gamma\left(\frac{u}{2}+p\right)}{\sqrt{\pi}\Gamma(v_1)\Gamma(v_2)\Gamma(p)(16\lambda_1^2\lambda_2^2q)^{\frac{u}{2}}u\bar{\gamma}^{\frac{u}{2}}}$$
$$+\sum_{k=1}^{\beta}\frac{2^{\alpha+k+v_1+v_2-7}g^2A\Gamma\left(\frac{|v_2-v_1|}{2}\right)\Gamma\left(\frac{|v_2-v_1|+1}{2}\right)\Gamma\left(\frac{u}{2}+p\right)}{\pi^{\frac{3}{2}}\Gamma(v_1)\Gamma(v_2)\Gamma(p)(16\lambda_1^2\lambda_2^2q)^{\frac{u}{2}}\Gamma\left(1-\frac{u}{2}\right)}$$
$$\times a_k\theta^{-\frac{\alpha+k}{2}}\left(\frac{\theta^2C}{16A_0^2}\right)^{\varrho_n}\left(\frac{1}{\bar{\gamma}}\right)^{\frac{u}{2}+\varrho_n}$$
$$\times\sum_{n=1}^{7}\frac{\prod_{j=1,j\neq n}^{7}\Gamma(\varrho_j-\varrho_n)\prod_{j=1}^{3}\Gamma(1-\varpi_j+\varrho_n)}{\prod_{j=4}^{5}\Gamma(\varpi_j-\varrho_n)\prod_{j=8}^{9}\Gamma(1-\varrho_j+\varrho_n)}. \tag{41}$$

As a double check, the DO is $G_d^s=\frac{u}{2}=\frac{1}{2}\min\{v_1,v_2\}$.

V. Numerical Results

In this part, the OP, ABER, and ACC performance of our proposed system are presented by using the derived results along with their corresponding simulation ones. In general, we set $\gamma_{th}=10$dB and $C=1.5$. For the BER analysis, we employ the differential phase shift keying (DPSK) modulation scheme, namely, $p=1$, $q=1$. Further, the parameters of the FSO link are set to: $\phi_A=\pi/2$, $\phi_B=0$, $\rho=0.1$, $b_0=0.8$, and $\Omega=1.5$.

In Fig. 2, the OP curves versus $\bar{\gamma}_1$ for our considered system when $\alpha=2$, $\beta=5$ and $g=12$ are plotted, where $\bar{\gamma}_2$ is set to 20dB. It is clearly observed that the analytical results and simulation results are well fitted and the asymptotic results approach to the exact ones at high SNRs. As N increases,

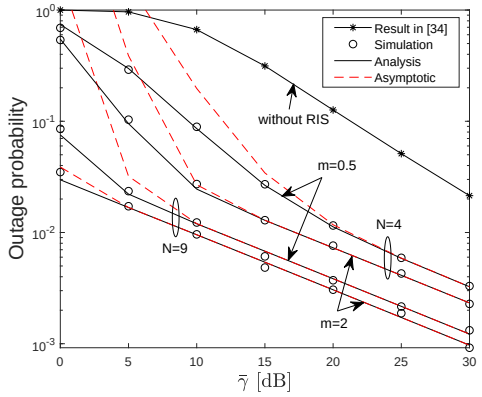

Fig 2. OP versus $\bar{\gamma}_1$ when $\alpha = 2$, $\beta = 5$, $g = 12$.

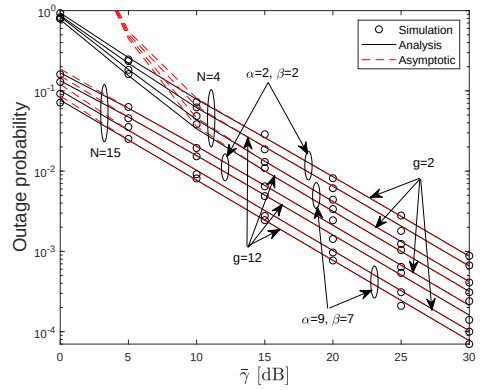

Fig 3. OP versus $\bar{\gamma}$ when $m = 2$.

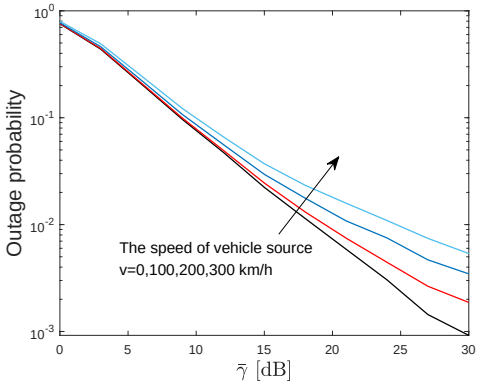

Fig 4. OP versus $\bar{\gamma}$ for different values of speed when $N = 4$, $m = 2$, $\alpha = 2$, $\beta = 5$ and $g = 12$.

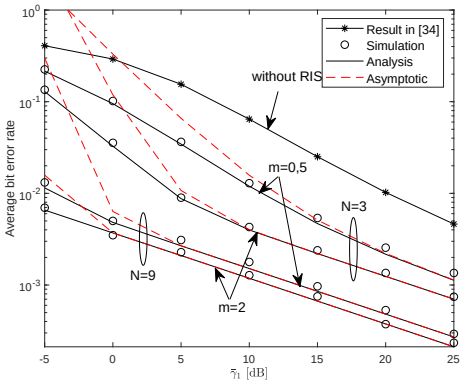

Fig 5. ABER versus $\bar{\gamma}_1$ when $\alpha = 2$, $\beta = 5$, $g = 12$.

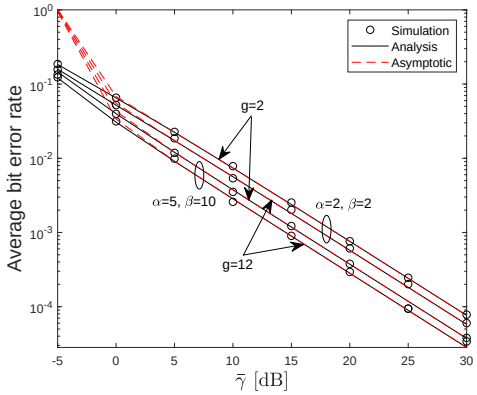

Fig 6. ABER versus $\bar{\gamma}$ when $N = 5$, $m = 2.5$.

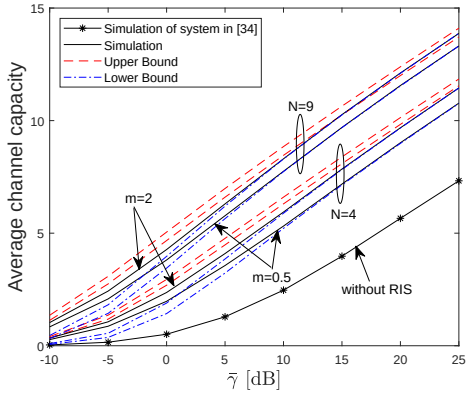

Fig 7. ACC versus $\bar{\gamma}$ when $\alpha = 2$, $\beta = 5$, $g = 12$.

the system outage performance becomes better. The principal reason is that large N results in a higher SNR at the relay. Moreover, compared to the system without the RIS [34], the OP with RISs is clearly small. It indicates that the RIS can dramatically enhance the system performance. On the other hand, one can see that the system performance corresponding to $m = 2$ is better than that for $m = 0.5$. This is because m is the parameter of Nakagami-m distribution. Thus, the larger the value of m, the weaker the fading on the RF link.

In Fig. 3, the OP curves versus $\bar{\gamma}$ when $m = 2$ are plotted, where $\bar{\gamma} = \bar{\gamma}_1 = \bar{\gamma}_2$. Recall that the value of α affects the number of large-scale fluctuations, while β is related to the number of small-scale fluctuations. Therefore, both values of α and β affect the amount of the fading of the FSO channel. Again, the analytical results fit well with the simulation ones. It can be observed that increasing the values of α , β, and g are able to enhance the outage performance. Similar to the insights obtained in Fig. 2, according to the definition of β, $1/\alpha$ and $1/\beta$ are the amounts of fading to quantify the severity of the fading experienced by the FSO channel. Therefore,

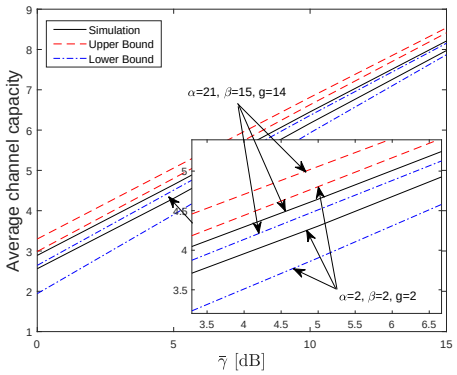

Fig 8. ACC versus $\bar{\gamma}$ when $N = 4$, $m = 2.5$.

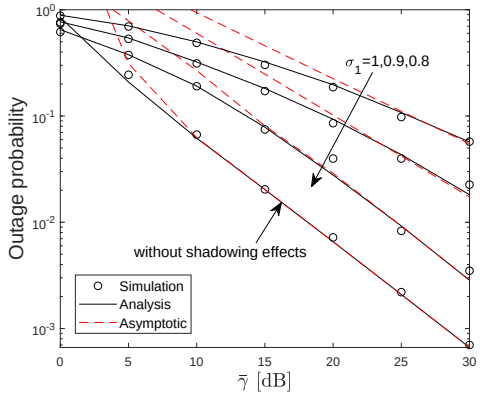

Fig 9. OP with and without shadowing effects versus $\bar{\gamma}$ when $N = 4$, $m = 2$, $\alpha = 2$, $\beta = 5$, $g = 12$.

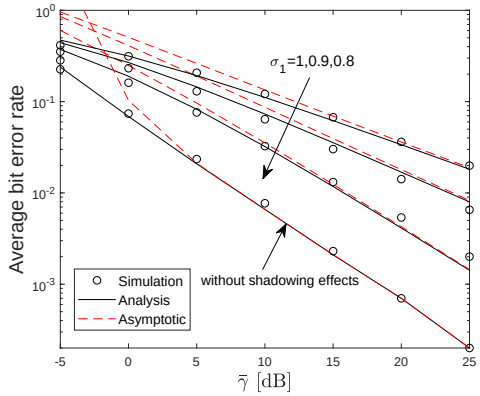

Fig 10. ABER with and without shadowing effects versus $\bar{\gamma}$ when $N = 4$, $m = 2$, $\alpha = 2$, $\beta = 5$, $g = 12$.

large values of α and β improve the system performance. Finally, one can see that the slopes of the curves are almost the same for different values of α, β, and g, which means that they have the same DOs and verifies the conclusion of the DO $G_d = \min\{k_w, m_w\}$. Thus, the achievable DO of our considered system is independent of the FSO link and only dependent on the RF link. As a double check, from both Fig. 2 and Fig. 3, we can find that the curves corresponding to small values of m and N have large slopes. The reason is that $G_d = \min\{k_w, m_w\}$, while m_w and k_w are related to N and m.

To observe the impact of mobility on system performance, the OP curves versus $\bar{\gamma}$ for different values of vehicle speed when $N = 4$, $m = 2$, $\alpha = 2$, $\beta = 5$ and $g = 12$ are plotted in Fig. 4, where $\bar{\gamma} = \bar{\gamma}_1 = \bar{\gamma}_2$. It can be seen that the larger the movement speed of ground vehicles, the higher the outage performance. This is because the mobility of the vehicle can cause Doppler frequency shift, thereby deteriorating system performance.

In Fig. 5, the BER curves versus $\bar{\gamma}_1$ when $\alpha = 2$, $\beta = 2$, $g = 12$ are plotted, while the BER performance when $\bar{\gamma} = \bar{\gamma}_1 = \bar{\gamma}_2$, $N = 5$ and $m = 2.5$ is plotted in Fig. 6. Again, the analytical results and simulation results are well matched and the asymptotic results are close to the analytical results at high SNRs. Similar to Fig. 2 and 3, it is revealed that increasing the values of N, m, α, β and g can improve the BER performance. Besides, similar conclusions as those gained in Fig. 2 and 3 can be attained.

In Fig. 7 and Fig. 8, the upper and lower bounds on the ACC when $\bar{\gamma}_1 = \bar{\gamma}_2 = \bar{\gamma}$ are plotted. As predicted, the upper and lower bounds are approach to the exact ones. Furthermore, at high SNRs, the lower bounds are very close to the simulation results. Similarly, using RIS and large values of N, m, α, β, and g can result in a large capacity.

In Fig. 9 and Fig. 10, the OP and ABER curves of the system with the shadowing effects in the RF channels are plotted when $N = 4$, $m = 2$, $\alpha = 2$, $\beta = 5$, $g = 12$, and $\bar{\gamma}_1 = \bar{\gamma}_2 = \bar{\gamma}$. Likewise, the analytical results and simulation results are well matched and the asymptotic results are close to the analytical results at high SNRs. As can be seen in the figures, as the value of the shadowing parameter σ_1 increases, the performance of the system deteriorates. This is because σ_1 is the quantity used to quantify the severity of the shadowing effects. The larger the value of σ_1, the more severe the shadowing effects experienced by the signal.

VI. Conclusion

In this work, a dual-hop satellite-vehicle network with the aid of a UAV was proposed. In fact, it is a mixed RF-FSO system. For such a scheme, we presented a comprehensive performance analysis including the OP, ABER, and ACC. Results showed that applying the RIS is able to significantly enhance the system performance. In addition, the shadowing effects can significantly degrade the system performance. Moreover, the DO of our considered system was only dependent on the RF link.

References

[1] F. Zhou, X. Li, M. Alazab, R. H. Jhaveri and K. Guo, "Secrecy performance for RIS-based integrated satellite vehicle networks with a UAV relay and MRC eavesdropping," *IEEE Trans. Intelligent Vehi.*, vol. 8, no. 2, pp. 1676-1685, Feb. 2023.

[2] K. Guo, X. Li, M. Alazab, R. H. Jhaveri and K. An, "Integrated satellite multiple two-way telay networks: Secrecy performance under multiple eves and vehicles with non-ideal hardware," *IEEE Trans. Intelligent Vehi.*, vol. 8, no. 2, pp. 1307-1318, Feb. 2023.

[3] S. Gu, X. Sun, Z. Yang, T. Huang, W. Xiang and K. Yu, "Energy-aware coded caching strategy design with resource optimization for satellite-UAV-vehicle-integrated networks," *IEEE Internet Things J.*, vol. 9, no. 8, pp. 5799-5811, 15 April, 2022.

[4] E. Basar, M. Di Renzo, J. De Rosny, M. Debbah, M. -S. Alouini and R. Zhang, "Wireless communications through reconfigurable intelligent surfaces," *IEEE Access*, vol. 7, pp. 116753-116773, 2019.

[5] N. Agrawal, A. Bansal, K. Singh and C. -P. Li, "Performance evaluation of RIS-assisted UAV-enabled vehicular communication system with multiple non-identical interferers," *IEEE Trans. Intell. Transp. Syst.*, vol. 23, no. 7, pp. 9883-9894, July 2022.

[6] A. Bansal, N. Agrawal and K. Singh, "Rate-splitting multiple access for UAV-based RIS-enabled interference-limited vehicular communication system," *IEEE Trans. Intelligent Vehi.*, vol. 8, no. 1, pp. 936-948, Jan. 2023.

[7] M. Alsenwi, M. Abolhasan and J. Lipman, "Intelligent and reliable millimeter wave communications for RIS-aided vehicular networks," *IEEE Trans. Intell. Transp. Syst.*, vol. 23, no. 11, pp. 21582-21592, Nov. 2022.

[8] L. Yang, J. Chen, M. O. Hasna and H. -C. Yang, "Outage performance of UAV-assisted relaying systems with RF energy harvesting," *IEEE Commun. Lett.*, vol. 22, no. 12, pp. 2471-2474, Dec. 2018.

[9] L. Yang, F. Meng, J. Zhang, M. O. Hasna and M. D. Renzo, "On the performance of RIS-assisted dual-hop UAV communication systems," *IEEE Trans. Veh. Technol.*, vol. 69, no. 9, pp. 10385-10390, Sept. 2020.

[10] S. Li, L. Yang, D. B. da Costa and S. Yu, "Performance analysis of UAV-based mixed RF-UWOC transmission systems," *IEEE Trans. Commun.*, vol. 69, no. 8, pp. 5559-5572, Aug. 2021.

[11] M. Baldi et al., "End-to-end simulations of coded transmissions in space links affected by solar scintillation," *IEEE Trans. Aerao. Elec. Sys.*, vol. 56, no. 4, pp. 3259-3275, Aug. 2020.

[12] M. A. Khalighi and M. Uysal, "Survey on free space optical communication: A communication theory perspective," *IEEE Commun. Surveys Tuts.*, vol. 16, no. 4, pp. 2231-2258, 4th Quart., 2014.

[13] S. Shah, M. Siddharth, N. Vishwakarma, R. Swaminathan and A. S. Madhukumar, "Adaptive-combining-based mixed FSO/RF satellite communication with and without HAPS," *IEEE Access*, vol. 9, pp. 81492-81511, 2021.

[14] S. Li, L. Yang, J. Zhang, P. S. Bithas, T. A. Tsiftsis and M. -S. Alouini, "Mixed THz/FSO relaying systems: Statistical analysis and performance evaluation," *IEEE Trans. Wireless Commun.*, vol. 21, no. 12, pp. 10996-11010, Dec. 2022.

[15] Chiung-Jang Chen and Li-Chun Wang, "Enhancing coverage and capacity for multiuser MIMO systems by utilizing scheduling," *IEEE Trans. Wireless Commun.*, vol. 5, no. 5, pp. 1148-1157, May 2006.

[16] K. P . Peppas, "Accurate closed-form approximations to generalised-K sum distributions and applications in the performance analysis of equal gain combining receivers," *IET Commun.*, vol. 5, no. 7, pp. 982-989, May 2011.

[17] H. Samimi and M. Uysal, "End-to-end performance of mixed RF/FSO transmission systems," *J. Opt. Commun. Netw.*, vol. 5, no. 11, pp. 1139-1144, Nov. 2013.

[18] A. Jurado-Navas, J. M. Garrido-Balsells, J. F. Paris, and A. Puerta-Notario, "Impact of pointing errors on the performance of generalized atmospheric optical channels," *Opt. Express*, vol. 20, no. 11, pp. 12550-12562, 2012.

[19] G.-C Rota, *Generalized hypergeometric functions with applications in statistics and physical sciences: A. M. Mathai and R. K. Saxena, Springer*, 1973, 314 pp, Advances in Mathematics, Volume 18, Issue 3, 1975.

[20] Wolfram, *The Wolfram Functions Site*. [Online]. Available: http: //functions.wolfram.com.

[21] S. Li and L. Yang, "Performance analysis of dual-hop THz transmission systems Over α-μ fading channels with pointing errors," *IEEE Internet Things J.,*, vol. 9, no. 14, pp. 11772-11783, 15 July15, 2022.

[22] I. S. Gradshteyn and I. M. Ryzhik, *Table of Integrals, Series, and Products*, 7th ed. San Diego, CA, USA: Academic, 2007.

[23] H. Shin and J. Lee, "Capacity of multiple-antenna fading channels: Spatial fading correlation, double scattering and keyhole," *IEEE Trans. Inf. Theory*, vol. 49, no. 10, pp. 2636-2647, Oct. 2003.

[24] X. W. Cui and Z. M. Feng, "Lower capacity bound for MIMO correlated fading channels with keyhole," *IEEE Commun. Lett.*, vol. 8, no. 8, pp. 500-502, Aug. 2004.

[25] A. P. Prudnikov, Y. A. Brychkov, and I. Marichev, *Integrals and Series.Philadelphia*, PA, USA: Gordon Breach Sci., 1986.

[26] M. Abdel-Hafez and M. Safak, "Performance analysis of digital cellular radio systems in Nakagami fading and correlated shadowing environment," *IEEE Trans. Veh. Technol.*, vol. 48, no. 5, pp. 1381-1391, Sept. 1999.

[27] B. M. Hochwald, T. L. Marzetta and V. Tarokh, "Multiple-antenna channel hardening and its implications for rate feedback and scheduling," *IEEE Trans. Inform. Theory.*, vol. 50, no. 9, pp. 1893-1909, Sept. 2004.

[28] N. Bouhlel and A. Dziri, "Maximum likelihood parameter estimation of Nakagami-Gamma shadowed fading channels," *IEEE Commun. Lett.*, vol. 19, no. 4, pp. 685-688, April 2015.

[29] M. Jani, P. Gargt, and A. Gupta, "Performance analysis of a mixed cooperative PLC-VLC system for indoor communication systems," *IEEE Syst. J.*, vol. 14 , no. 1, pp. 469-476, Jan. 2020.

[30] D. Ben Cheikh, J. M. Kelif, M. Coupechoux, and P. Goldewski, "SIR distribution analysis in cellular networks considering the joint impact of path-loss, shadowing and fast fading," *EURASIP J. Wireless Commun. Netw.*, vol. 2011, pp. 1-10, Oct. 2011,

[31] L. B. Kumar, R. P. Naik, P. Krishnan, A. A. B. Raj, A. K. Majumdar and W. -Y. Chung, "RIS assisted triple-hop RF-FSO convergent with UWOC system," *IEEE Access*, vol. 10, pp. 66564-66575, 2022.

[32] T. Hossain, S. Shabab, A. S. M. Badrudduza, M. K. Kundu and I. S. Ansari, "On the physical layer security performance over RIS-aided dual-hop RF-UOWC mixed network," *IEEE Trans. Veh. Technol.*, vol. 72, no. 2, pp. 2246-2257, Feb. 2023.

[33] L. Yang, P. Li, F. Meng and S. Yu, "Performance analysis of RIS-assisted UAV communication systems," *IEEE Trans. Veh. Technol.*, vol. 71, no. 8, pp. 9078-9082, Aug. 2022.

[34] L. Yang and M. O. Hasna, "Performance analysis of amplify-and-forward hybrid satellite-terrestrial networks with cochannel interference," *IEEE Trans. Commun.*, vol. 63, no. 12, pp. 5052-5061, Dec. 2015.

Shutong Wang was born in Shandong, China. He received the B.S. degree from Nanjing University of Posts and Telecommunications, Nanjing, China, in 2020. He is currently working toward the M.S. degree at the College of Computer Science and Electronic Engineering, Hunan University, Changsha, China. His current research interests include the performance analysis of wireless communications systems.

Liang Yang was born in Hunan, China. He received the Ph.D. degree in electrical engineering from Sun Yat-sen University, Guangzhou, China, in 2006. From 2006 to 2013, he was a faculty with Jinan University, Guangzhou, China. He joined the Guangdong University of Technology in 2013. Now he is a professor at Hunan University, Changsha, China. His current research interests include the performance analysis of wireless communications systems.

Xingwang Li (S'12-M'15-SM'20) received the M. Sc. and Ph. D. degrees from University of Electronic Science and Technology of China and Beijing University of Posts and Telecommunications in 2010 and 2015. From 2010 to 2012, he worked at Comba Telecom Ltd. In Guangzhou China, as an engineer. He spent one year from 2017 to 2018 as a visiting scholar at Queen's University Belfast, Belfast, UK. He is currently an Associated Professor with the School of Physics and Electronic Information Engineering, Henan Polytechnic University, Jiaozuo China. His research interests span wireless communication, intelligent transport system, artificial intelligence, Internet of things.

Dr. Li has served as many TPC members, such as the IEEE Globecom, IEEE ICC, IEEE WCNC, IEEE VTC, IEEE ICCC etc. He has also served as the Co-Chair for the IEEE/IET CSNDSP 2020 of the Green Communications and Networks Track. He also serves as an Editor on the Editorial Board for IEEE Transactions on Intelligent Transportation Systems, IEEE Transactions on Vehicular Technology, IEEE Systems Journal, Physical Communication. He was the Guest Editor for the special issue on Computational Intelligence and Advanced Learning for Next-Generation Industrial IoT of IEEE Transactions on Network Science and Engineering, "Recent Advances in Physical Layer Technologies for 5G-Enabled Internet of Things" of the Wireless Communications and Mobile Computing. He has served as many TPC members, such as IEEE ICC, GLOBECOM, WCNC, VTC, ICCC, etc. He is also the Co-Chair of IEEE/IET CSNDSP 2020 of the Green Communications and Networks track.

Kefeng Guo received his B.S. degree from Beijing Institute of Technology, Beijing, China in 2012, and the Ph.D. degree in Army Engineering University, Nanjing, China in 2018. He is a Lecturer in School of Space Information, Space Engineering University. He is also the associate professor in the College of Electronic and Information Engineering, Nanjing University of Aeronautics and Astronautics. He has authored or coauthored nearly 70 research papers in international journals and conferences. His research interests focus on cooperative relay networks, MIMO communications systems, multiuser communication systems, satellite communication, hardware impairments, cognitive radio, NOMA technology and physical layer security. He was a recipient of exemplary Reviewer for **IEEE Transactions on Communications** in 2022. He was the recipient of the Outstanding Ph.D. Thesis Award of Chinese Institute of Command and Control in 2020. He also was the recipient of the Excellent Ph.D. Thesis Award of Jiangsu Province, China in 2020. He also serves as an Editor on the Editorial Board for the **EURASIP Journal on Wireless Communications and Networking**. He was the Guest Editor for the special issue on Integration of Satellite-Aerial-Terrestrial Networks of **Sensors** , also the Guest Editor for the special issue on Recent Advances and Challenges of Satellite and Aerial Communication Networks of **Electronics** .

Dr. Guo has been the TPC member of many IEEE sponsored conferences, such as IEEE ICC, IEEE GLOBECOM and IEEE WCNC.

Hongwu Liu (Senior Member, IEEE) received the Ph.D. degree from Southwest Jiaotong University in 2008. From 2008 to 2010, he was a faculty with Nanchang Hangkong University. From 2010 to 2011, he was a Post-Doctoral Fellow with the Shanghai Institute of Microsystem and Information Technology, Chinese Academy of Science. From 2011 to 2013, he was a Research Fellow with the UWB Wireless Communications Research Center, Inha University, South Korea. Since 2014, he has been an Associate Professor with Shandong Jiaotong University. His research interests include MIMO signal processing, cognitive radios, cooperative communications, and AI-based wireless communications.

Houbing Song (M'12-SM'14-F'23) received the Ph.D. degree in electrical engineering from the University of Virginia, Charlottesville, VA, in August 2012. He is currently a Tenured Associate Professor, the Director of the NSF Center for Aviation Big Data Analytics (Planning), the Associate Director for Leadership of the DOT Transportation Cybersecurity Center for Advanced Research and Education (Tier 1 Center), and the Director of the Security and Optimization for Networked Globe Laboratory (SONG Lab, www.SONGLab.us), University of Maryland, Baltimore County (UMBC), Baltimore, MD. Prior to joining UMBC, he was a Tenured Associate Professor of Electrical Engineering and Computer Science at Embry-Riddle Aeronautical University, Daytona Beach, FL. He serves as an Associate Editor for IEEE Transactions on Artificial Intelligence (TAI) (2023-present), IEEE Internet of Things Journal (2020-present), IEEE Transactions on Intelligent Transportation Systems (2021-present), and IEEE Journal on Miniaturization for Air and Space Systems (J-MASS) (2020-present). He was an Associate Technical Editor for IEEE Communications Magazine (2017-2020). He is the editor of eight books, the author of more than 100 articles and the inventor of 2 patents. His research interests include cyber-physical systems/internet of things, cybersecurity and privacy, and AI/machine learning/big data analytics. His research has been sponsored by federal agencies (including National Science Foundation, National Aeronautics and Space Administration, US Department of Transportation, and Federal Aviation Administration, among others) and industry. His research has been featured by popular news media outlets, including IEEE GlobalSpec's Engineering360, Association for Uncrewed Vehicle Systems International (AUVSI), Security Magazine, CXOTech Magazine, Fox News, U.S. News & World Report, The Washington Times, and New Atlas. Dr. Song is an IEEE Fellow (for contributions to big data analytics and integration of AI with Internet of Things), and an ACM Distinguished Member (for outstanding scientific contributions to computing). He is an ACM Distinguished Speaker (2020-present) and an IEEE Vehicular Technology Society (VTS) Distinguished Lecturer (2023-present).

Dr. Song has been a Highly Cited Researcher identified by Clarivate^{TM} (2021, 2022) and a Top 1000 Computer Scientist identified by Research.com. He received Research.com Rising Star of Science Award in 2022 (World Ranking: 82; US Ranking: 16). Dr. Song was a recipient of 10+ Best Paper Awards from major international conferences, including IEEE CPSCom-2019, IEEE ICII 2019, IEEE/AIAA ICNS 2019, IEEE CBDCom 2020, WASA 2020, AIAA IEEE DASC 2021, IEEE GLOBECOM 2021 and IEEE INFOCOM 2022.

Rutvij H. Jhaveri (Senior Member, IEEE) is an experienced educator and researcher working in the Department of Computer Science & Engineering, Pandit Deendayal Energy University, Gandhinagar, India. He conducted his Postdoctoral Research at Delta-NTU Corporate Lab for Cyber-Physical Systems, Nanyang Technological University, Singapore. He completed his PhD in Computer Engineerng in 2016. In 2017, he was awarded with prestigious Pedagogical Innovation Award by Gujarat Technological University. Currently, he is co-investigating a funded project from GUJCOST. He was ranked among top 2% s5ientists around the world in 2021. He has 2200+ Google Scholar citations with h-index 25. Apart from serving as an editor/ guest editor in various journals of repute, he also serves as a reviewer in several international journals and also as an advisory/TPC member in renowned international conferences. He authored 125+ articles including the IEEE/ACM Transactions and flagship IEEE/ACM conferences. Moreover, he has several national and international patents and, copyrights to his name. He also possesses memberships of various technical bodies such as ACM, CSI, ISTE, IDES and others. He is a member of the Advisory Board in Symbiosis Institute of Digital and Telecom Management, Manav Rachna Group and Sandip University since 2022. He is an editorial board member in several Hindawi and Springer journals. He also served as a committee member in "Smart Village Project" - Government of Gujarat, at the district level during the year 2017. His research interests are Cyber Security, IoT systems, SDN and Smart Healthcare.